IEEE Access
Multidisciplinary | Rapid Review | Open Access Journal

Date of publication xxxx 00, 0000, date of current version xxxx 00, 0000.

Digital Object Identifier 10.1109/ACCESS.2017.Doi Number

A New Control Interaction Phenomenon in Large-Scale Type-4 Wind Park

L. Meng[1], (Student member, IEEE), U. Karaagac[1], (Member, IEEE), M. Ghafouri[2], (Member, IEEE), A. Stepanov[3], (Member, IEEE), J. Mahseredjian[3], (Fellow, IEEE), K. W. Chan[1], (Member, IEEE), and I. Kocar[1], (Senior Member, IEEE)

[1]Department of Electrical and Electronic Engineering, Hong Kong Polytechnic University, Hung Hom, Kowloon, Hong Kong
[2]Concordia Institute for Information Systems Engineering, Concordia University, Montreal, QC, Canada
[3]Department of Electrical Engineering, Polytechnique Montréal, Montreal, QC, Canada

Corresponding author: U. Karaagac (e-mail: ulas.karaagac@polyu.edu.hk).

This work was supported by the Hong Kong Research Grant Council for the Research Project under Grant 25223118.

ABSTRACT This paper demonstrates the risk of a new control interaction phenomenon between a large-scale type-4 wind park (WP) and a 500 kV transmission grid at super-synchronous frequency range. This study aims at (i) using the impedance-based stability assessment (IBSA) method to investigate this new interaction phenomenon; and (ii) analyzing the impact of various transmission grid topologies, WP operating conditions as well as wind turbine (WT) converter control parameters on the severity of the interaction. For ultimate accuracy, the frequency-dependent impedance characteristics of the WP are extracted using the electromagnetic transient (EMT)-type impedance scanning instead of simplified analytical model. The performed analyses demonstrate that the WP generation capacity, length of the transmission lines, applied series and shunt compensation levels, presence of parallel lines, and grid side converter (GSC) control parameters of the WT, can significantly affect the identified control interaction risk. The obtained results are validated through detailed EMT simulations. Although the type-4 WP is considered in this paper, the presented results can be generalized to any inverter-based resource (IBR) with full-size converter (FSC), such as photovoltaic (PV) power stations.

INDEX TERMS Control interaction, full size converter, series compensation, shunt compensation, super-synchronous oscillation, transmission system, wind turbine

I. INTRODUCTION

The penetration level of wind and solar energy as well as the size of their generation units have dramatically increased in recent years. Recent incidents have shown that the photovoltaic (PV) inverters and grid side converter (GSC) of type-4 wind turbines (WTs) can adversely interact with the weakly tied AC grids at sub-synchronous frequency range [1]. This phenomenon, is called weak grid sub-synchronous oscillation (SSO) [2].

In Texas, a type-4 wind park (WP) experienced weak grid SSO at 4 Hz in 2011 after one of the two parallel transmission lines connecting the WP to a strong grid was taken out of service [3]. In Hami area of China, type-4 WPs experienced a weak grid SSO at 20 Hz in 2015 following an increase in WPs' output active power [4]. Large-scale WPs in Hami area of China were connected to the main grid with long transmission lines, which created a weak grid condition. Other weak grid SSO events include 3.5 Hz oscillations in Hydro One's type-4 WPs [5], 9 Hz oscillations in an offshore WP of Great Britain [6], 22 Hz oscillations in PV power station of Dominion Energy in the eastern U.S. [7], and 7 Hz oscillations in First Solar's California PV power station [8].

The weak grid SSO mechanism was initially explained by circuit analysis as a power transfer problem [9]. When the reference value for the active power output of the grid inverter increases, the inverter output currents also increase. This leads to a larger voltage drop on equivalent grid impedance and the inverter active power output decreases. The instability occurs due to the imbalance between the inverter output active power and the associated reference value. Based on this mechanism, a damping controller was designed to weaken the couplings between the inverter active power and the voltage outputs [10]. The inverter controls also have significant impacts on the weak grid SSO. Initially, the phase-locked loop (PLL)

parameters were found as the major reason in Texas and Hami area of China events, and modification of PLL parameters was recommended for mitigation in [11]. Then impedance-based stability analysis (IBSA) brings new insights to the weak grid SSO issue [4], [12]. The IBSA explains the instability as a resonance circuit formed by the grid inverter and the weak grid, and it can be displayed in the R-X diagram analysis [13], [14] or Bode diagram analysis [15]. The impacts of PLL, inner and outer control loops, decoupling, and voltage feedforward terms on the impedance characteristics of grid inverter are analyzed in [12]. The weak grid SSO typically occurs when the inductive grid and capacitive IBR impedances form a resonance with negative total resistance.

The IBSA method usage in IBR related stability problems gained popularity due to its simplicity and computational effectiveness [12]-[17]. Desired accuracy can be achieved when frequency-dependent impedance of the IBR is extracted using EMT-type impedance scanning instead of simplified analytical models. This method also allows extracting impedance characteristics of black-box or grey-box devices [13], [14], [16], [17].

For the first time, this paper identifies a resonance condition that occurs between large-scale type-4 WP and a 500 kV transmission grid case at super-synchronous frequency range. Transmission line charging capacitances, shunt and series compensation levels play a critical role in the identified resonance. It should be emphasized that the weak grid SSO studies in the literature ignores the shunt branches (except the shunt harmonic filter of the grid inverter) as the external grid is typically represented with its Thevenin equivalent. The identified resonant frequency is at super-synchronous range; hence, it is called super-synchronous oscillation (SupSO) in this paper. Detailed analysis demonstrates that transmission line length, applied series and shunt compensation levels, presence of parallel lines, WP generation capacity, and WT grid side converter (GSC) control parameters play important roles on the identified SupSO risk. The photovoltaic (PV) inverters and GSC of type-4 WTs have similar structure. Hence, the presented results and drawn conclusions are also valid for PV solar plants. Based on the authors' knowledge, it is the first study in this regard.

The rest of this paper is arranged as follows. Section II briefly presents the type-4 WP model. The considered system and identified SupSO problem are introduced in Section III. Sections IV, V and VI investigate the impact of transmission grid, GSC control parameters and WP operating conditions on SupSO, respectively. Finally, Section VI concludes the paper.

II. TYPE-4 WIND TURBINE MODEL

The considered type-4 WT consists of a permanent magnet synchronous generator (PMSG) and a back-to-back converter. The converter system consists of two voltage source converters: a machine side converter (MSC) and a GSC. A resistive chopper provides dc bus overvoltage protection. A line inductor (choke filter) and an ac shunt harmonic filter are used at the GSC end to improve the power quality. The type-4 WTs are connected to medium-voltage (MV) feeders through WT transformers, and these feeders form the MV collector grid that transfers the power from WTs to the point of interconnection (PoI) through a WP transformer.

Both MSC and GSC are controlled by a two-level controller. The slow outer control loop calculates the reference values for currents in dq-frame. The fast inner loop (current) controller, on the other hand, produces the converter voltage reference. MSC often operates at unity power factor and controls the active power through a maximum power point tracking (MPPT) algorithm. As its impact on SupSO is negligible, this converter is not presented due to space limitation.

The simplified GSC control diagram is depicted in Fig. 1 [19]. The d- and q-axis currents of GSC (i_d and i_q) are used to control the dc bus voltage (V_{dc}) and positive sequence ac terminal voltage (V_{ac}), respectively. The primed variables indicate the reference values coming from controllers. The quantities in Fig. 1 and this section are per unit. The controller for ac voltage is a proportional regulator, whose reference value ($V'_{ac} = 1 + \Delta V'_{ac}$) is adjusted by the wind park controller (WPC) to achieve the desired reactive power at the PoI. A typical setting for the ac voltage regulator is $K_V = 2$.

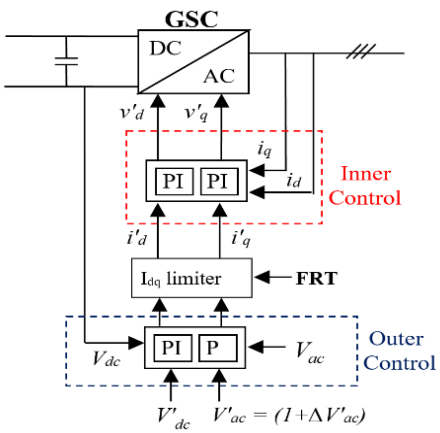

FIGURE 1. Simplified GSC control diagram.

The dc voltage controller is a proportional-integral (PI) regulator and tuned based on inertia emulation, with

$$K_{p-dc} = \omega_0^2 \left(2H_{C-dc}\right), \quad K_{i-dc} = 2\xi\omega_0 \left(2H_{C-dc}\right) \quad (1)$$

where ω_0 is the natural frequency of the closed-loop system, and ξ=0.707 is the damping factor; $H_{C\text{-}dc}$ is the static moment of inertia and it has

$$H_{C-dc} = E_{C-dc} / S_{WT} \quad (2)$$

where E_{Cdc} is the stored energy in dc bus capacitor (in Joules) and S_{WT} is the WT rated power (in VA). $K_{p\text{-}dc}$ and $K_{i\text{-}dc}$ are calculated for the desired time constant of a simplified second order system

$$\tau_{dc} = 3/\xi\omega_0 \tag{3}$$

The GSC controller gives the priority to the active current during normal operation and the reactive current during severe voltage sag and swell conditions (fault-ride-through (FRT) operation) for grid compliant operation.

The link between GSC output current and voltage can be described by a transfer function

$$G(s) = 1/\left(R_\Sigma + sL_\Sigma\right) \tag{4}$$

where $Z_\Sigma = R_\Sigma + j\omega L_\Sigma$ represents the total series impedance between the aggregated GSC terminal and the external high voltage (HV) system Thevenin source. The PI parameters of inner current controllers are designed using the internal model control (IMC) method [18], [19],

$$K_{p-i} = \alpha_c L_\Sigma\,, \quad K_{i-i} = \alpha_c R_\Sigma \tag{5}$$

where α_c is the set bandwidth. $K_{p\text{-}i}$ and $K_{i\text{-}i}$ can be calculated for the desired GSC rise time ($t_{r\text{-}gsc}$) using the relationship between a first-order system bandwidth and 10%-90% rise time [18],

$$t_{r-gsc} = \ln(9)/\alpha_c \tag{6}$$

Readers can refer to [19] for details of control parameter settings and EMT model of the considered type-4 WP. In EMT model, the MV collector grid and type-4 WTs are represented with their aggregated models, but the overall control structure of the WP is preserved. The type-4 WT and WP control system include the non-linearities, necessary transient and protection functions. Moreover, it allows the simulation of WPs' accurate transient behavior when they are subjected to external power system disturbances.

III. SYSTEM UNDER STUDY AND THE IDENTIFIED SUPER-SYNCHRONOUS OSCILATION

A. THE SYSTEM UNDER STUDY

The system shown in Fig. 2 was originally developed based on a practical system and was used for investigating SSI problems of series compensated type-3 WPs [13], [20]. The type-3 WTs are replaced with type-4 WTs in this research. The large-scale WP consists of 400 WTs and is connected to two large systems, i.e., System-1 and System-2, through Line-1 and Line-2. Line-1 is series compensated with 50% compensation level (CL) by two identical capacitor banks located at its ends. Two 230 MVAR identical shunt reactors are also installed at both ends of Line-1 to provide 75% shunt compensation. On the other hand, Line-2 is short (100 km); thus, it does not contain any shunt or series compensation.

The converters are represented with their average value models (AVMs) and the simulation time step is 50 μs in all EMT simulations using EMTP [21]. Line-1 and Line-2 are represented with distributed constant parameter (CP) models. The wind park operates at rated wind speed and unity power factor.

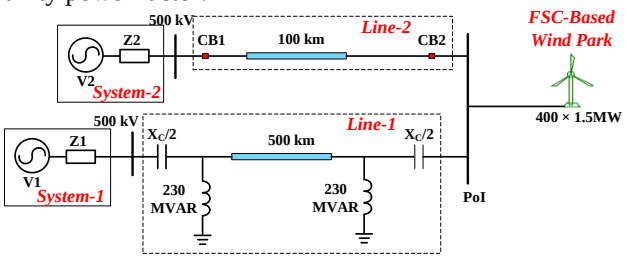

FIGURE 2. The system under study.

B. SUPER-SYNCHRONOUS RESONANCE PHENOMENON

Line-2 is disconnected at t=4 s (at perfect steady-state conditions) by opening the circuit-breaker CB2, leaving the wind park radially connected to Line-1. Following this outage, growing oscillation appears immediately as shown in Fig. 3. As seen in Fig. 4, both the GSC voltage and current waveforms contain 21 Hz and 99 Hz components, which form a symmetrical pair around the synchronous frequency. The super-synchronous frequency component is larger compared to the sub-synchronous one especially in voltage waveform.

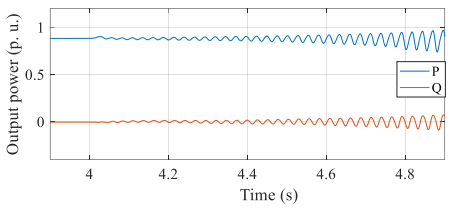

FIGURE 3. GSC active and reactive power outputs.

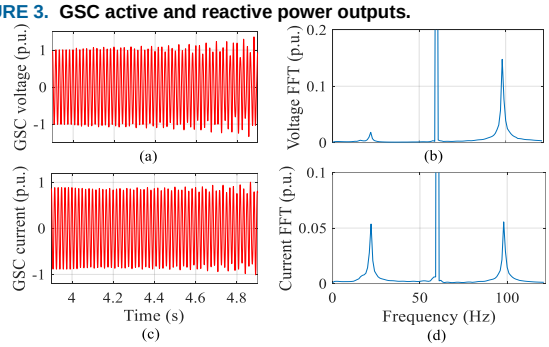

FIGURE 4. GSC voltage and current and their frequency spectra (phase-a).

As illustrated in the following subsection, the resonance takes place at super-synchronous frequency, and the sub-synchronous frequency component appears due to the mirror frequency effect (MFE) [22]. It should be noted that when the SupSO occurs at a frequency larger than twice of the synchronous frequency, its mirror coupling oscillation frequency becomes negative (i.e. the phase sequence of the oscillation is opposite).

C. INVESTIGATION OF THE SUPER-SYNCHRONOUS OSCILLATION

The 500 kV transmission grid frequency-dependent impedance is obtained using a phasor solution based impedance scanning tool that is available in EMT simulators [23]. The WP frequency-dependent impedance is obtained through EMT-type impedance scanning using voltage sinusoidal perturbations with an amplitude of 0.02 p.u. The frequency responses of the WP and transmission grid (when Line-2 is disconnected) for 1-1000 Hz frequency range are shown in Fig. 5. $Z_{WP\text{-}pos}$ and $Z_{WP\text{-}neg}$ are the WP impedances in positive and negative sequences, respectively. The grid side positive and negative sequence impedances are equivalent (Z_{Grid}).

As seen in Fig. 5, the transmission grid contains numerous parallel resonances generated by the transmission line charging capacitors and series inductors. These parallel resonances may interact with WP at intersection points, where $|Z_{WP}(f)| = |Z_{Grid}(f)|$, and lead to instability [24]. Stability at these intersections is assessed based on the Bode plot analysis criteria as presented in Table I [25].

For the intersection point at 101.5 Hz, the phase difference between grid and WP impedances (φ_{Grid} - φ_{WP}) is close to -180° (-179.9°). Such a small phase margin (PM), i.e., -0.1°, indicates a critical unstable condition. Other intersection points are stable with large phase margins regardless of the inductive or capacitive behavior of WP (or grid) as both the WP and grid have positive resistances. The frequencies of impedance interaction points are called crossover frequencies (f_C) in this paper. As seen in Fig. 5, the SupSO problem would be more severe if the parallel resonance of grid shifted leftward or the WP had a larger admittance value.

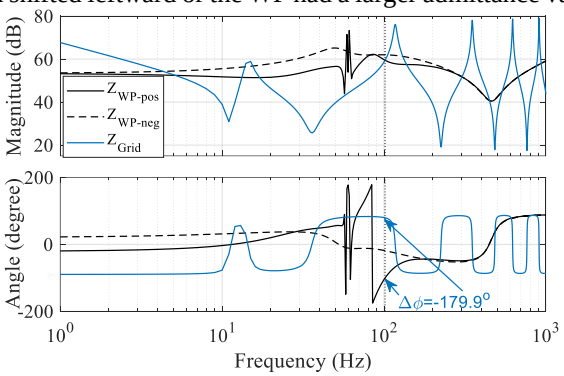

FIGURE 5. Impedance responses of the WP and transmission grid.

Impact factors of both grid side and WP side will be investigated in the following sections. As the system is safe from the negative sequence control interaction issue, only the positive sequence impedance based analyses will be conducted in this paper. Although the usage of single-input single-output (SISO) positive sequence impedance may lead to small discrepancies in the obtained resonance frequency and PM, these discrepancies can be neglected while analyzing parameter variations impact on system stability trend. Additionally, the positive sequence impedance gives insight into the impedance characteristics of WP and instability mechanism.

TABLE I
BODE PLOT ANALYSIS CRITERIA AT CROSSOVER FREQUENCY

Rate of change of $\lvert Z_{Grid}(f_C)\rvert / \lvert Z_{WP}(f_C)\rvert > 0$	$\varphi_{Grid} - \varphi_{WP} > -180°$	Unstable
	$\varphi_{Grid} - \varphi_{WP} < -180°$	Stable
Rate of change of $\lvert Z_{Grid}(f_C)\rvert / \lvert Z_{WP}(f_C)\rvert < 0$	$\varphi_{Grid} - \varphi_{WP} > -180°$	Stable
	$\varphi_{Grid} - \varphi_{WP} < -180°$	Unstable

IV. IMPACT OF TRANSMISSION GRID ON SupSO

This section investigates the impact of shunt and series CLs, compensation schemes, transmission line length, and presence of parallel lines on the identified instability issue. The impact of different transmission line models on identification of SupSO is also investigated.

A. TRANSMISSION LINE SERIES AND SHUNT COMPENSATION LEVELS

The considered variations in series and shunt CLs are presented in Table II with the associated IBSA results (i.e. crossover frequencies and PMs). As seen in Fig. 6, a decrease in either series or shunt CL increases the grid impedance magnitude ($|Z_{Grid}|$) and results in a decrease in the crossover frequency. As the change in grid impedance angle (φ_{Grid}) is marginal, the PM decreases significantly due to the change in WP impedance angle (φ_{WP}) as seen in Fig. 6 and Table II. EMT simulations in Fig. 7 confirm the IBSA results. In the considered 500 kV test system, smaller series and/or shunt CLs make the system more vulnerable to SupSO.

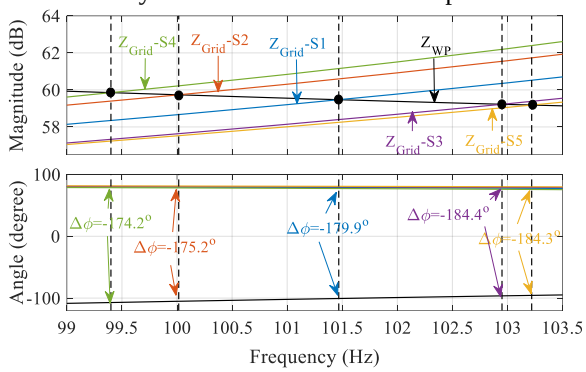

FIGURE 6. Impact of transmission line series and shunt CLs.

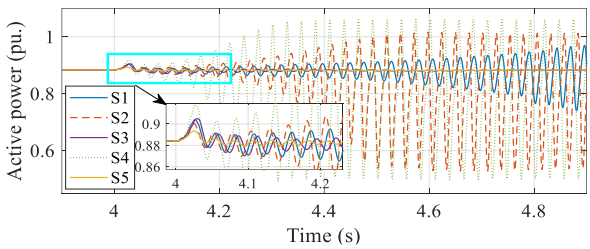

FIGURE 7. GSC active power outputs, Scenarios S1-S5.

TABLE II
IMPACT OF TRANSMISSION LINE COMPENSATION LEVELS

Scenario	S1	S2	S3	S4	S5
Series CL	50%	30%	70%	50%	50%
Shunt CL	75%	75%	75%	55%	95%
f_C (Hz)	101.5	100	103	99.4	103.2
PM	-0.1°	-4.8°	4.4°	-5.8°	4.3°

B. TRANSMISSION LINE LENGTH AND PARALLEL LINES

The IBSA results for different Line-1 lengths are presented in Table III and Fig. 8. The series and shunt CLs of Line-1 are modified considering its length to maintain the constant series inductance and charging capacitance levels. As seen in Fig. 8, the grid parallel resonance frequency increases significantly with the decrease in Line-1 length. Such an increase results in a larger crossover frequency and PM as presented in Table III. The SupSO risk is reduced when the WP is radially connected to System-1 with a shorter transmission line.

When the WP is connected to System-1 via identical parallel lines, the shunt resonance frequency of the grid decreases significantly (see Fig. 9) as the increase in equivalent shunt charging capacitance is more significant compared to the decrease in equivalent series inductance. The presence of parallel 500 kV lines increases the SupSO risk as seen in Table IV.

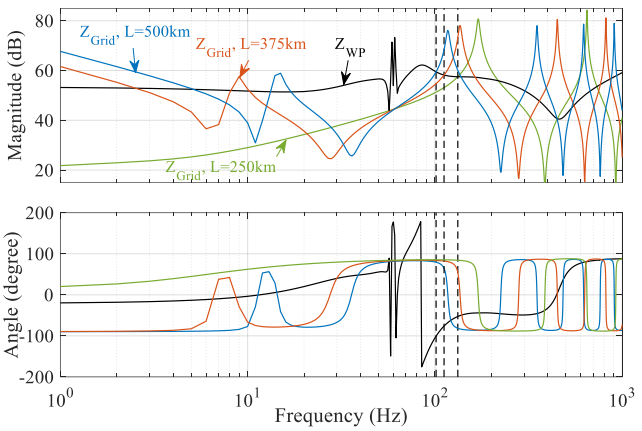

FIGURE 8. Impact of transmission line length (see Table III for f_C and PM).

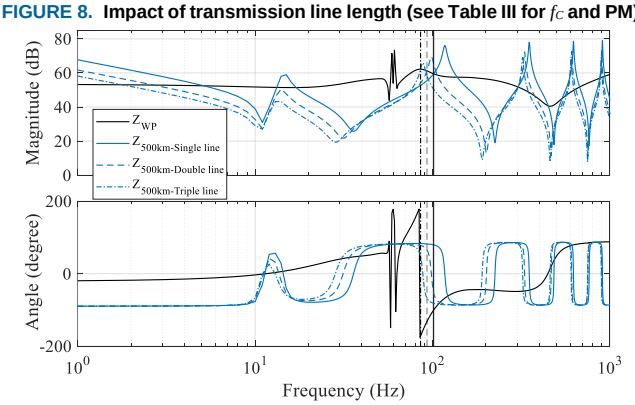

FIGURE 9. Impact of parallel transmission lines (see Table IV for f_C and PM).

TABLE III
IMPACT OF TRANSMISSION LINE LENGTH

Scenario	Length	Series CL	Shunt CL	f_C	PM
S1	500km	50%	75%	101.5 Hz	-0.1°
S6	375km	33.3%	66.6%	111.9 Hz	21.6°
S7	250km	-	50%	132.5 Hz	42.9°

TABLE IV
IMPACT OF PARALLEL TRANSMISSION LINES

Line	500km 2-lines	500km 3-lines	375km 2-lines	375km 3-lines	250km 2-lines	250km 3-lines
f_C (Hz)	93.0	85.6	101.5	92.8	116.0	104.3
PM	-17.4°	-39.2°	6.0°	-30.6°	31.7°	15.1°

C. SERIES AND SHUNT COMPENSATION SCHEMES

Some of the typical transmission line shunt and series compensation schemes are presented in Table V, and their impedance characteristics are shown in Fig. 10. (a). It can be learned that the compensation schemes affect the equivalent grid impedance characteristics $Z_{Grid}(f)$ mainly at low frequency range. Hence, its impact on the SupSO instability is marginal. The IBSA results in Table VI and EMT simulations in Fig. 10 (b) confirm this observation. On the other hand, usage of simplified transmission line models, namely, representing the distributed CP line model by a PI-equivalent circuit or a series RLC branch (defined as configurations d and e, respectively) has significant impact on the IBSA result.

TABLE V
SERIES AND SHUNT COMPENSATION SCHEMES OF TRANSMISSION LINE

No.	Configuration	No.	Configuration
(a)	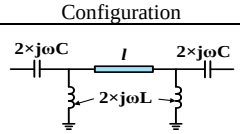	(b)	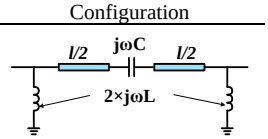
(c)	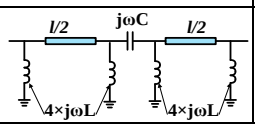		

TABLE VI
IMPACT OF COMPENSATION SCHEMES AND TRANSMISSION LINE MODELS

Configuration	*a*	*b*	*c*	*d*	*e*
f_C (Hz)	101.5	99.4	99.8	100.2	182.9
PM	-0.1°	-0.4°	-0.2°	-5.0°	47.9°

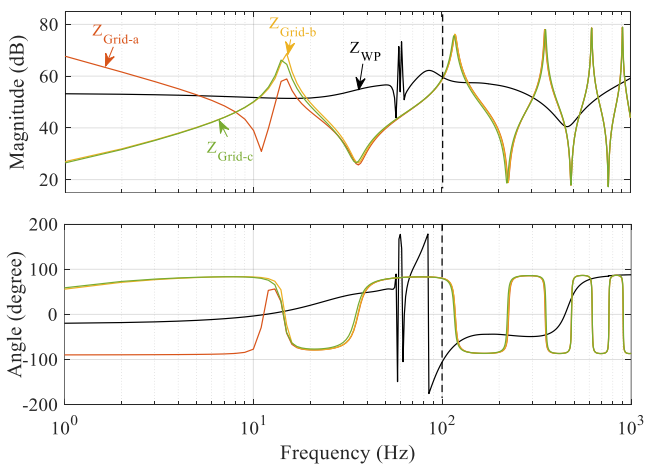

(a) $Z_{Grid}(f)$ (configurations a - c) and $Z_{WP}(f)$, see Table VI for f_C and PM.

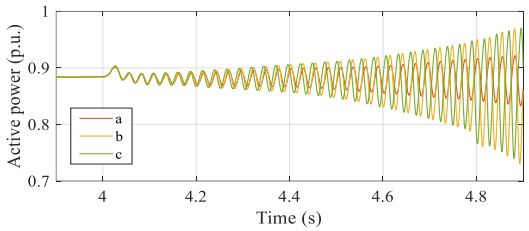

(b) GSC active power outputs (for configurations a - c)

FIGURE 10.Impact of transmission line series and shunt compensation schemes.

Usage of PI-equivalent and series RLC representations mainly changes the impedance characteristics of the transmission line from middle to high frequency range (from one hundred to thousands of Hz). As shown in Table VI, the accuracy of using the PI-equivalent model can be considered as acceptable, whereas using the series RLC branch fails to capture the instability as expected. As the line charging capacitances and shunt compensation reactors play important roles on the identified SupSO, it is inappropriate to simply classify this problem as a weak grid instability.

V. IMPACT OF GSC CONTROL ON THE SupSO

A. IMPACT OF GSC INNER CONTROL LOOP PARAMETERS

The GSC rise time $t_{r\text{-}gsc}$ (see (6)) in S1 is 6 ms and is modified within its typical setting range (2.5 to 10 ms). The length variations of Line-1 given in Table III are also considered. Definitions of the considered scenarios and corresponding IBSA results are presented in Table VII and Table VIII. Decreasing $t_{r\text{-}gsc}$ significantly reduces wind park's resistance in the frequency range of interest (see Fig. 11), thereby reducing the system PM. For $t_{r\text{-}gsc}$ = 2.5 ms, all considered scenarios become unstable. In scenario 19 (250 km transmission line), the crossover frequency even exceeds the double fundamental frequency, and the mirror coupling component in this scenario is a negative sequence signal of 12.2 Hz. For $t_{r\text{-}gsc}$ = 7.5 ms and above, all scenarios of the considered transmission line variations are stable. The EMT simulations presented in Fig. 12 confirm the IBSA results in Table VIII.

TABLE VII
SCENARIOS FOR ILLUSTRATING GSC RISE TIME IMPACT

$t_{r\text{-}gsc}$ / Length	10 (ms)	7.5 (ms)	5 (ms)	2.5 (ms)
500 (km)	S8	S9	S10	S11
375 (km)	S12	S13	S14	S15
250 (km)	S16	S17	S18	S19

TABLE VIII
CROSSOVER FREQUENCY AND PHASE MARGIN OF S8-S19

Scenario	S8	S9	S10	S11
f_C (Hz)	101.4	101.2	101.9	103.5
PM	54.9°	23.7°	-17°	-58°
Scenario	S12	S13	S14	S15
f_C (Hz)	114.4	112.5	112	114.9
PM	66.3°	45.4°	5.6°	-35.1°
Scenario	S16	S17	S18	S19
f_C (Hz)	140.3	135.8	130.7	132.2
PM	68.7°	56.8°	29.5°	-12.6°

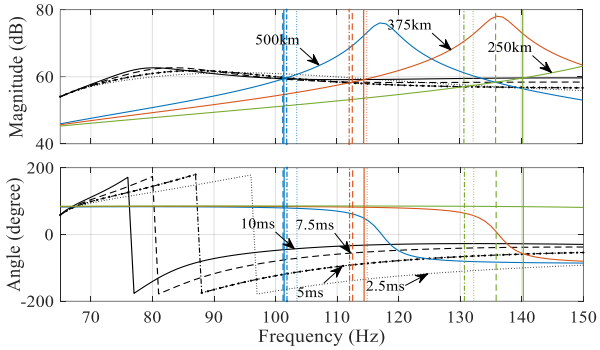

FIGURE 11.Impact of GSC rise time (see Table VIII for f_C and PM).

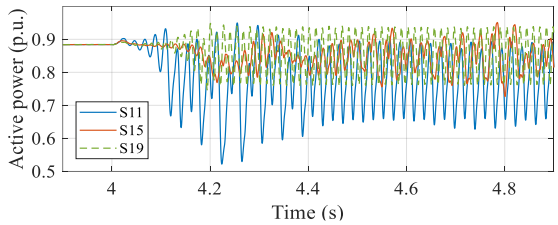

(a) $t_{r\text{-}gsc}$ = 2.5 ms **(scenarios S11, S15 and S19).**

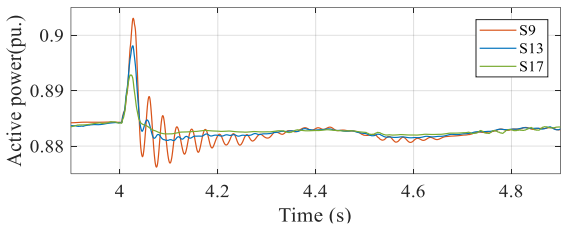

(b) $t_{r\text{-}gsc}$ = 7.5 ms **(scenarios S9, S13 and S17).**

FIGURE 12. GSC active power outputs for different $t_{r\text{-}gsc}$.

B. IMPACT OF GSC OUTER CONTROL LOOP PARAMETERS

1) DC VOLTAGE REGULATOR PARAMETERS

The dc voltage regulator parameters affect the frequency response of GSC especially at 60 Hz - 120 Hz frequency range as seen from Fig. 13 (a). Like the GSC current regulator, decreasing the dc voltage regulator response time decreases the wind park resistance. This results in a decrease in PM of the system as well (see Table IX). However, its impact is much smaller compared to the GSC current regulator. The EMT simulation results shown in Fig. 13 (b) confirm the presented IBSA results in Table IX.

2) IMPACT OF VOLTAGE REGULATOR GAIN

Increasing the ac voltage regulator gain (K_V) decreases the wind park resistance significantly as seen from Fig. 14 (a), and results in a significant decrease in PM of the system (see Table X). The EMT simulation results shown in Fig. 14 (b) confirm the IBSA results.

According to new German grid code [19], ac voltage regulator gain setting range should be $2 \leq K_V < 6$. Usage of large K_V values may make the system very vulnerable to the SupSO even for large GSC rise time settings.

TABLE IX
IMPACT OF WT GSC DC-VOLTAGE REGULATOR TIME CONSTANT

Scenario	S20	S1	S21	S22
τ_{dc} (ms)	75	150	250	400
f_C (Hz)	100.8	101.5	101.8	101.9
PM	-15.5°	-0.1°	4.8°	7.2°

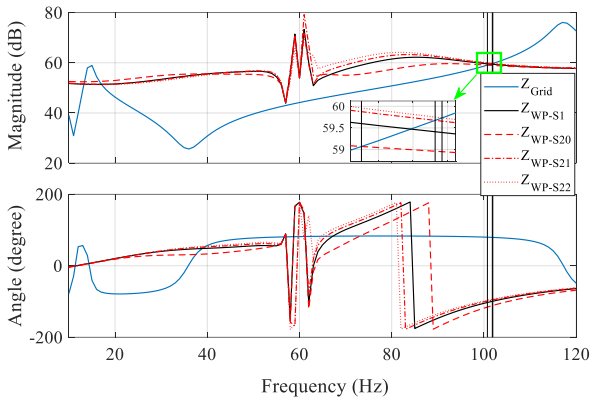

(a) $Z_{Grid}(f)$ and $Z_{WP}(f)$ with different τ_{dc} (see Table IX for f_C and PM).

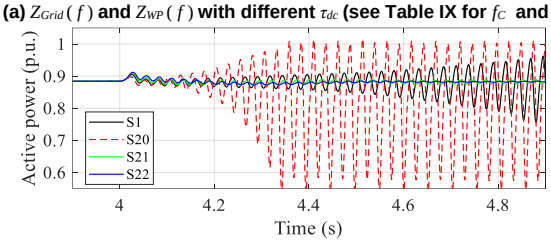

(b) GSC active power outputs in scenarios S1, S20 - S22

FIGURE 13. Impact of dc voltage regulator time constant.

TABLE X
IMPACT OF GSC AC VOLTAGE REGULATOR PARAMETER

Scenario	S23	S1	S24
K_V	1	2	3
f_C (Hz)	100.7	101.5	98.1
PM	40.9°	-0.1°	-49.8°

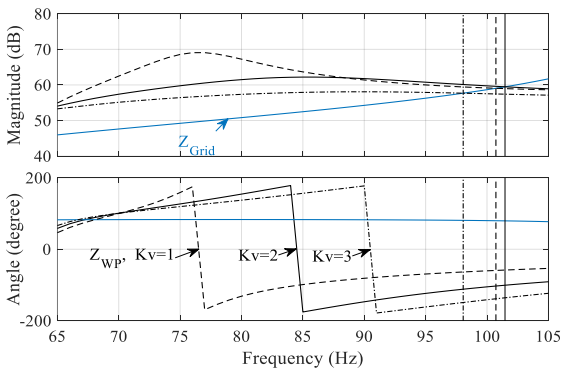

(a) $Z_{Grid}(f)$ and $Z_{WP}(f)$ with different K_V (see Table X for f_C and PM).

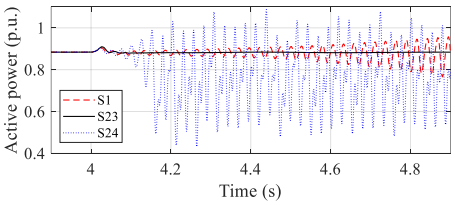

(b) GSC active power outputs in scenarios S1, S23, and S24.

FIGURE 14. Impact of GAC ac voltage regulator parameter.

VI. IMPACT OF WP OPERATING CONDITIONS ON the SupSO

A. IMPACT OF WT OUTAGES AND WP INSTALLED CAPACITY

The number of installed and in-service WTs in the WP (N_i and N_S, respectively) are given in Table XI. As seen in Fig. 15 (a), with the increase of WT outages, the impedance magnitude of WP increases almost proportionally, while the phase angle remains almost unchanged in the super-synchronous range. This leads the interaction point of the system shifting to larger frequency where the WP has larger resistance. The WP becomes less vulnerable to the SupSO when more WTs are out of service. EMT simulations shown in Fig. 15 (b) confirms the IBSA results. If the installed capacity was smaller, we would observe again larger WP impedance due to reduced number of WTs (even more compared to WT outage scenarios due to decreased size of WP transformer). Larger size WP is expected to be more vulnerable to the SupSO.

TABLE XI
IMPACT OF WT OUTAGE AND THE NUMBER OF INSTALLED WTS

Scenario	S1	S25	S26
N_i	400	400	400
N_S	400	300	200
f_C (Hz)	101.5	104.6	110.7
PM	-0.1°	10.4°	33.6°

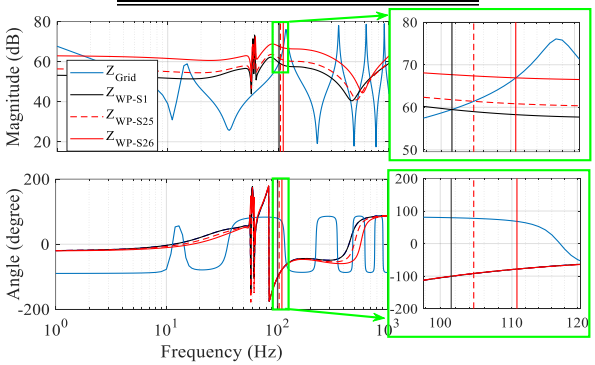

(a) $Z_{Grid}(f)$ and $Z_{WP}(f)$ (see Table XI for f_C and PM).

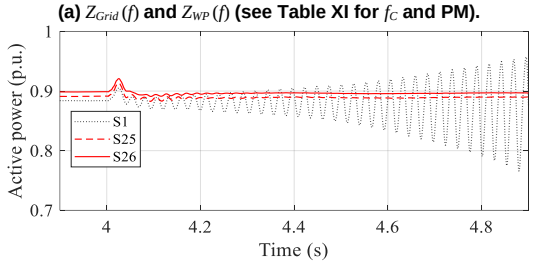

(b) GSC active power outputs in scenarios S1, S25 and S26

FIGURE 15. Impact of WT outages.

B. IMPACT OF WP ACTIVE AND REACTIVE POWER GENERATION

The impact of WP reactive power generation and wind speed (i.e., WP active power generation) are marginal as presented in Table XII and Table XIII. The increase in either reactive power generation or wind speed slightly increases the stability margin. The IBSA results are confirmed with EMT simulations shown in Fig. 16.

TABLE XII
IMPACT OF WP REACTIVE POWER

Scenario	S27	S28	S1	S29	S30
Q (p.u.)	-0.2	-0.1	0	0.1	0.2
f_C (Hz)	101.1	101.3	101.5	101.7	101.9
PM	-3.8°	-2.1°	-0.1°	1.0°	2.5°

TABLE XIII
IMPACT OF WIND SPEED

Scenario	S1	S31	S32
WS (p.u.)	1	0.8	0.6
f_C (Hz)	101.5	100.8	100.2
PM	-0.1°	-2.4°	-3.2°

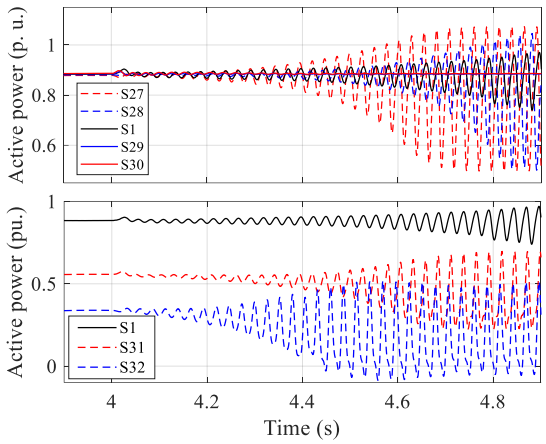

FIGURE 16.GSC active power outputs in scenarios S1, S27 - S32.

VII. CONCLUSION

This paper identified a SupSO risk for a large-scale type-4 WP radially connected to 500 kV grid through a long transmission line. The grid side impedance contains several parallel and series resonances formed by the transmission line charging capacitances and series inductances. The parallel resonance that interacts with the WP in 60-180 Hz frequency range causes instability where the negative resistance of the WP has a larger magnitude compared to grid resistance. As both the grid and WP have positive resistances at other frequency ranges, instability is not expected.

The parallel resonance frequency of the transmission grid is significantly affected by the line length, applied shunt and series compensation levels. For the considered 500 kV test system, the SupSO risk is more severe for a longer transmission line with lower shunt and series compensation levels. Additionally, presence of parallel lines significantly increases the instability risk. To identify the potential SupSO risk, the transmission lines should be represented at least with their PI-equivalent models.

The WP is more vulnerable to the SupSO while operating with slowest wind speed and largest possible capacitive reactive power generation. However, the WP operating condition has marginal impact compared to the GSC control parameters. GSC with either a fast inner loop response speed or a large ac voltage regulator gain induce high SupSO risk. The SupSO risk in a smaller-scale WP (with smaller installed capacity or WT outages) is smaller.

When a SupSO risk is detected, the response speed of the inner control loop and/or the ac voltage regulator gain can be reduced for mitigation as long as an acceptable transient response to voltage sags and swells is maintained.

As the PV inverters and GSC of type-4 WTs have similar structure, the presented results and drawn conclusions are also valid for PV solar plants.

REFERENCES

[1] Y. Cheng et al., "Real-World Subsynchronous Oscillation Events in Power Grids with High Penetrations of Inverter-Based Resources," IEEE Trans. Power Syst., vol. 38, no. 1, pp. 316-330, Jan. 2023.

[2] IEEE-PES Wind SSO Task Force, "Wind energy systems sub-synchronous oscillations: events and modeling," *Technical Report, PES-TR80*, AMPS Committee, July 2020.

[3] S.-H. Huang, J. Schmall, J. Conto, J. Adams, Yang Zhang, and C. Carter, "Voltage control challenges on weak grids with high penetration of wind generation: ERCOT experience," in *2012 IEEE Power and Energy Society General Meeting*, Jul. 2012, pp. 1–7.

[4] H. Liu, X. Xie, J. He, T. Xu, Z. Yu, C. Wang, and C. Zhang, "Subsynchronous Interaction Between Direct-Drive PMSG Based Wind Farms and Weak AC Networks," *IEEE Trans. Power Syst.*, vol. 32, no. 6, pp. 4708–4720, Nov. 2017

[5] C. Li and R. Reinmuller, "Asset Condition Anomaly Detections by Using Power Quality Data Analytics," in *2019 IEEE Power & Energy Society General Meeting (PESGM)*, Aug. 2019, pp. 1–5.

[6] National Grid ESO, "Technical Report on the events of 9 August 2019," 2019.

[7] Dominion Energy, "Identifying Oscillations Injected by Inverter-Based Solar Energy Sources in Dominion Energy's Service Territory using Synchrophasor Data and Point-on-Wave Data," Apr. 2021.

[8] First Solar, "Deploying Utility-Scale PV Power Plants in Weak Grids," Jun. 2017.

[9] L. Fan and Z. Miao, "An explanation of oscillations due to wind power plants weak grid interconnection," *IEEE Trans. Sustain. Energy*, vol. 9, no. 1, pp. 488–490, Jan. 2018.

[10] Y. Li, L. Fan, and Z. Miao, "Stability Control for Wind in Weak Grids," *IEEE Trans Sustain Energy*, vol. 10, no. 4, pp. 2094–2103, Oct. 2019.

[11] L. Fan and Z. Miao, "Wind in Weak Grids: 4 Hz or 30 Hz Oscillations?," *IEEE Trans. Power Syst.*, vol. 33, no. 5, pp. 5803–5804, Sept. 2018.

[12] H. Liu and X. Xie, "Comparative Studies on the Impedance Models of VSC-Based Renewable Generators for SSI Stability Analysis," IEEE Trans. Energy Convers., vol. 34, no. 3, pp. 1442–1453, Sept. 2019.

[13] U. Karaagac, J. Mahseredjian, S. Jensen, R. Gagnon, M. Fecteau, and I. Kocar, "Safe Operation of DFIG-Based Wind Parks in Series-Compensated Systems," *IEEE Trans. Power Deliv.*, vol. 33, no. 2, pp. 709–718, Apr. 2018.

[14] Y. Cheng, M. Sahni, D. Muthumuni and B. Badrzadeh, "Reactance Scan Crossover-Based Approach for Investigating SSCI Concerns for DFIG-Based Wind Turbines," *IEEE Trans. Power Deliv.*, vol. 28, no. 2, pp. 742-751, Apr. 2013.

[15] J. Sun, "Impedance-Based Stability Criterion for Grid-Connected Inverters," *IEEE Trans Power Electron*, vol. 26, no. 11, pp. 3075–3078, Nov. 2011.

[16] B. Badrzadeh et al., "General methodology for analysis of sub-synchronous interaction in wind power plants, " IEEE Trans. Power Syst., vol. 28, no. 2, pp. 1858-1869, May 2013.

[17] A. S. Trevisan, Â. Mendonça, R. Gagnon, J. Mahseredjian and M. Fecteau, "Analytically validated SSCI assessment technique for wind parks in series compensated grids," *IEEE Trans. Power Syst.*, vol. 36, no. 1, pp. 39-48, Jan. 2021.

[18] L. Harnefors, H. P. Nee, "Model-based current control of ac machines using the internal model control," in *IEEE Trans. Ind. Appl.* vol. 34, no. 1, pp. 133-141, Jan./Feb. 1998.
[19] U. Karaagac, J. Mahseredjian, R. Gagnon, H. Gras, H. Saad, L.n Cai, I. Kocar, A. Haddadi, E. Farantatos, S. Bu, K.n Chan, and L. Wang, "A generic EMT-type simulation model for wind parks with permanent magnet synchronous generator full size converter wind turbines," *IEEE Power Energy Technol. Syst. J.*, vol. 6, no. 3, pp. 131-141, Sept. 2019.
[20] M. Ghafouri, U. Karaagac, J. Mahseredjian and H. Karimi, "SSCI damping controller design for series-compensated DFIG based wind parks considering implementation challenges," *IEEE Trans. Power Syst.*, vol. 34, no. 4, pp. 2644-2653, July 2019.
[21] J. Mahseredjian, S. Dennetière, L. Dubé, B. Khodabakhchian and L. Gérin-Lajoie, "On a new approach for the simulation of transients in power systems," *Electric Power Systems Research*, vol. 77, no. 11, pp. 1514-1520, 2007.
[22] A. Rygg, M. Molinas, C. Zhang, and X. Cai, "A Modified Sequence-Domain Impedance Definition and Its Equivalence to the dq-Domain Impedance Definition for the Stability Analysis of AC Power Electronic Systems," *IEEE J. Emerg. Sel. Topics Power Electron.*, vol. 4, no. 4, pp. 1383–1396, Dec. 2016.
[23] "Reader's guide to subsynchronous resonance," IEEE Trans. Power Syst. vol. 7, no.1, pp.150-157, 1992.
[24] M. Céspedes and J. Sun, "Modeling and mitigation of harmonic resonance between wind turbines and the grid," *IEEE Energy Conversion Congress and Exposition*, Phoenix, AZ, USA, 2011, pp. 2109-2116.
[25] Y. Liao and X. Wang, "General Rules of Using Bode Plots for Impedance-Based Stability Analysis," 2018 IEEE 19th Workshop on Control and Modeling for Power Electronics (COMPEL), pp. 1-6, 2018.

LEI MENG (Student Member, IEEE) received her B.S. and M.S. degrees form the Northeastern University, China in control theory and control technology and electrical engineering in 2016 and 2019, respectively. Currently, she is a Ph.D. candidate in the department of Electrical and Electronic Engineering, Hong Kong Polytechnic University, Hong Kong SAR, China. Her research interest focuses on the control interaction issue between inverter-based resources and transmission grid.

ULAS KARAAGAC (Member, IEEE) received the B.Sc. and M.Sc. degrees in electrical and electronics engineering from the Middle East Technical University, Ankara, Turkey, in 1999 and 2002, respectively, and the Ph.D. degree in electrical engineering from Polytechnique Montréal, Montreal, QC, Canada, in 2011. He was a Research and Development Engineer with the Information Technology and Electronics Research Institute (BILTEN), Scientific and Technical Research Council of Turkey (TUBITAK), from 1999 to 2007. He was also a Postdoctoral Fellow with Polytechnique Montréal, from 2011 to 2013, and a Research Associate, from 2013 to 2016. In 2017, he joined the Department of Electrical Engineering, The Hong Kong Polytechnic University, as a Research Assistant Professor. His research interests include integration of large-scale renewables into power grids, modeling and simulation of large-scale power systems, and power system dynamics and control.

MOHSEN GHAFOURI (Member, IEEE) received the B.Sc. and master's degrees in electrical engineering from the Sharif University of Technology, Tehran, Iran, in 2009 and 2011, respectively, and the Ph.D. degree in electrical engineering from Polytechnique Montréal, Montreal, QC, Canada, in 2018. He was a Researcher with the Iranian Power System Research Institute, Sharif University of Technology, from 2011 to 2014. In 2018, he was a Researcher with CYME International, Eaton Power System Solutions, Montreal. In August 2018, he joined as the Horizon Postdoctoral Fellow with the Security Research Group, Concordia University, where he is currently an Assistant Professor. His research interests include cybersecurity of smart grids, power system modeling, microgrid, wind energy, and control of industrial processes.

ANTON STEPANOV received the Engineer's degree in electrical and power systems from South Ural State University, Chelyabinsk, Russia, in 2013, the M.Sc. degree in electronic systems and electrical engineering from Ecole Polytechnique de l'Université de Nantes, Saint-Nazaire, France, in 2015, and the Ph.D. degree in electrical engineering from Polytechnique Montréal, Montréal, QC, Canada, in 2020.,From 2017 to 2020 he was the recipient of the Vanier Canada Graduate Scholarship. In 2020, he joined PGSTech, Canada, as an R&D Specialist. His research interests include HVDC systems modeling, analysis, and simulation.

JEAN MAHSEREDJIAN (Fellow, IEEE) received the M.A.Sc. and Ph.D. degrees from Polytechnique Montréal, Montréal, QC, Canada, in 1985 and 1991, respectively. From 1987 to 2004, he was with IREQ (Hydro-Quebec), working on research and development activities related to the simulation and analysis of electromagnetic transients. In December 2004, he joined the Faculty of Electrical Engineering with Polytechnique Montréal, where he is currently a Professor.

KA WING CHAN (Member, IEEE) received the B.Sc. (Hons.) and Ph.D. degrees in electronic and electrical engineering from the University of Bath, Bath, U.K., in 1988 and 1992, respectively. He is currently an Associate Professor and the Associate Head of the Department of Electrical Engineering with The Hong Kong Polytechnic University, Hong Kong. His general research interests include power system stability, analysis and control, power grid integration, security, resilience and optimization, and demand response management.

ILHAN KOCAR (Senior Member, IEEE) received the B.Sc. and M.Sc. degrees in EEE from Orta Doğu Teknik Üniversitesi, Ankara, Türkiye, in 1998 and 2003, respectively, and the Ph.D. degree in EE from the École Polytechnique de Montréal (affiliated with Université de Montréal), Montreal, QC, Canada, in 2009. He is currently a Professor with The Hong Kong Polytechnic University, Hong Kong. He has 20 years of experience with career highlights in research, development of computational tools for power system analysis, project engineering, and consulting. He is an Associate Editor for IEEE TRANSACTIONS ON POWER DELIVERY and JOURNAL OF MODERN POWER SYSTEMS AND CLEAN ENERGY.